

The effect of Taylor rolls on highly turbulent Taylor-Couette flow

RODOLFO OSTILLA - MÓNICO¹,
ROBERTO VERZICCO^{2,1},
SIEGFRIED GROSSMANN³, AND DETLEF LOHSE¹

¹Physics of Fluids, Mesa+ Institute, University of Twente, P.O. Box 217, 7500 AE Enschede, The Netherlands

²Dipartimento di Ingegneria Industriale, University of Rome “Tor Vergata”, Via del Politecnico 1, Roma 00133, Italy

³Department of Physics, University of Marburg, Renthof 6, D-35032 Marburg, Germany

(Received 3 December 2024)

Direct numerical simulations of the Taylor-Couette (TC) problem, the flow between two coaxial and independently rotating cylinders have been performed. Reynolds numbers of up to $3 \cdot 10^5$, corresponding to frictional Reynolds numbers $Re_\tau \approx 4000$ were reached. The gap between the cylinders was kept small by fixing the radius ratio to $\eta = r_i/r_o = 0.909$. Small gap TC was found to be dominated by large scale structures, which are permanent in time and known as Taylor rolls (TRs). TRs are attached to the boundary layer, and are active, i.e they transport angular velocity through Reynolds stresses. Evidence for the existence of logarithmic velocity fluctuations, and of an overlap layer where the velocity fluctuations collapse in outer units was also found. An externally imposed axial flow of comparable strength as the wind of the TRs was found to convect them without any weakening effect.

Key words:

1. Introduction

Direct numerical simulations (DNS) are a very versatile tool for the study of turbulence, and have led to deep insight on its nature in the last 30 years. The seminal work of Kim *et al.* (1987) began a line of simulations of wall-bounded flows which is very active in the present day. Kim *et al.* (1987) studied a particular kind of wall-bounded flow, namely pressure-driven (Poiseuille) flow bounded by two parallel plates, from now on referred to as channel flow. After this seminal work, which achieved $Re_\tau = 180$, simulations of wall-bounded flows focused mainly on channel flows, even if some attention was given to zero-pressure-gradient boundary layers (ZPGBL) and pipes. Present day simulations achieve much higher frictional Reynolds numbers: $Re_\tau = 4600$ for channels (Bernardini *et al.* 2014; Lozano-Durán & Jiménez 2014), $Re_\tau = 2000$ for ZPGBL (Sillero *et al.* 2013) and $Re_\tau \approx 1100$ for pipes (Wu & Moin 2008). DNS has allowed for detailed study of the near-wall energy cascade and for correlations between different canonical flows to be established. This has led to further understanding of the attached-eddy model of the logarithmic layer by Townsend (1976), further developed by Perry & Chong (1982); Perry *et al.* (1986). We refer the reader to Jimenez (2012) for a recent review of advances in this field.

DNS of *shear* driven flow between two parallel plates, i.e. plane Couette (PC) flow has been even more challenging. This is due to the extremely large and wide structures present in the turbulent flow, seen both experimentally and numerically (Bech *et al.* 1995). DNS of PC requires much larger computational boxes than that of channels, a factor 10 in both spanwise and streamwise directions. This meant that only this year $Re_\tau = 550$ was achieved by Avsarkisov *et al.* (2014) and more recently $Re_\tau \approx 1000$ (Pirozzoli *et al.* 2014). An alternative to having two independently moving parallel plates is having two independently *rotating coaxial cylinders*. Such system is known as cylindrical Couette flow or Taylor-Couette (TC) flow. TC is a closed system, which makes experimental realizations easier to construct. Furthermore, TC does not require the large computational boxes of PC, which makes higher Re_τ easier to achieve in DNS.

However, TC flow is fundamentally different from PC flow. Unlike PC (and all the flows mentioned previously) TC is linearly *unstable* if $(d(r^2\omega)/dr)^2 < 0$, where r is the radial coordinate and ω the angular momentum. Faisst & Eckhardt (2000) explored the transition from PC to TC, and found that only for radius ratios $\eta = r_i/r_o > 0.99$, where r_i and r_o are the inner and outer cylinder radii respectively, the sub-critical PC instabilities overcame the super-critical TC instabilities.

Therefore, adding a minute curvature to PC changes the flow properties drastically. Bradshaw (1973) was the first to note "the surprisingly large effect exerted on shear-flow turbulence by curvature of the streamlines in the plane of the mean shear", when studying boundary layers over curved surfaces. For curved channels Hunt & Joubert (1979) and Hoffmann *et al.* (1985) found that adding a very weak destabilizing (concave) curvature $d/R \sim 0.01$, where d is the boundary layer thickness and R the radius of curvature was found to produce significant differences in the mean and fluctuation velocity profiles. This is because destabilizing curvature adds a new mode of instability, which is reflected as Taylor-Görtler vortices in the flow and a change in the flow dynamics. We note that pipes are not a member of this group. The natural curvature of pipes is in planes perpendicular to the mean shear, so its effects are milder.

Both channel flow and TC have been used as a playground for investigating drag reduction through deformable bubbles or riblets (Choi *et al.* 1993; van den Berg *et al.* 2005; Lu *et al.* 2005; van Gils *et al.* 2013; Zhu *et al.* 2015). From the previous discussion, we would expect significant differences between both systems, but instead, very similar results were obtained. In both cases drag was reduced, and both the bubbles and riblets modified the boundary layer. This may be taken as an indication that as similar drag reduction mechanisms can be seen in both systems, the boundary layers in both systems may also be similar. Further evidence for such a universal behaviour was provided by recent experiments: Huisman *et al.* (2013) measured the mean velocity profiles in TC and obtained a von Karman constant $\kappa \approx 0.4$ for the highest Reynolds numbers achieved (with $Re_\tau \approx 30000$), in line with that seen in experimental pipes (Bailey *et al.* 2014). Outside the boundary layer, things change. The linear instability in TC causes the formation of large-scale structures, which fill the entire channel and are permanent in time. These are known as Taylor rolls, after the seminal work by Taylor (1936). Taylor rolls have been observed in both experiments and simulations, even up to $Re = 10^6$ (Huisman *et al.* 2014). If the Reynolds number is large enough, Taylor rolls play very little effect in determining the torque required to drive the cylinders (Ostilla-Monico *et al.* 2014b). However, their signature in the velocity field is still apparent, clearly appearing in the mean fields. An analogous structure which fills the entire domain and is persistent in time was also found in curved channels with fully developed turbulence: large scale Taylor-Görtler vortices (Hunt & Joubert 1979).

Many fundamental differences seem to exist between pipe & channel flows and TC

flow. In this manuscript we wish to further characterize the TC system in general, and in particular the effect of the Taylor rolls and of curvature. To do this, four high Reynolds number DNSs of TC flow were performed. All simulations were done for pure inner cylinder rotation, i.e. $\omega_o = 0$, and with an axial periodicity aspect ratio $\Gamma = L_z/d = 2\pi/3$, where L_z is the axial periodicity length. With this Γ , the system fits a single Taylor roll pair of wavelength $\lambda_{TR} = 2\pi/3$. We focus on $\eta = 0.909$ which has a mild enough curvature to make it linearly unstable, but small enough not to be dominated by streamline topology. Simulations at shear Reynolds numbers of $Re_s = d\omega_i/\nu = 10^5$, $Re_s = 2 \cdot 10^5$ and $Re_s = 3 \cdot 10^5$, were performed, where d is the gap-width $d = r_o - r_i$, ω_i and ω_o are the inner and outer cylinder angular velocity respectively, and ν is the kinematic viscosity of the fluid. This results in a frictional Reynolds numbers at the inner cylinder between $Re_{\tau,i} \sim 1000$ and $Re_{\tau,i} \sim 4000$. For TC, we define the inner cylinder frictional Reynolds number $Re_{\tau,i}$ as $Re_{\tau,i} = u_{\tau,i}d/(2\nu)$, where the frictional velocity is $u_{\tau,i} = \sqrt{\tau_{w,i}/\rho}$, with ρ the fluid density and τ_w the stress at the inner cylinder wall. The frictional Reynolds number at the outer cylinder is obtained from $Re_{\tau,o} \approx \eta Re_{\tau,i}$.

To probe the stability of the rolls to a transversal velocity, an additional simulation at $\eta = 0.909$ and $Re_s = 10^5$ with an imposed axial (spanwise) pressure gradient was performed. The pressure gradient resulted in an average axial velocity $U_w \approx \frac{1}{10}U_i$, where U_i is the inner cylinder velocity $U_i = r_i\omega_i$. This U_w is of the order of magnitude of the characteristic velocity of the Taylor rolls, but small enough so that the system dynamics is not dominated by this secondary flow.

The manuscript is organized as follows. Chapter 2 presents the numerical setup, and details the simulations. Chapter 3 presents the results and discussions. The findings are summarized in the final Chapter, and an outlook for future work is given.

2. Numerical details

The DNS were performed using a second order centred finite difference scheme with fractional-time stepping (Verzicco & Orlandi 1996). This scheme has been used and validated extensively in the context of TC (cf. comparison to experiments in Ostilla-Monico *et al.* (2014a,b)). In order to perform the simulations at high Reynolds numbers, following Brauckmann & Eckhardt (2013) “small” computational boxes were used. Instead of simulating the full azimuthal extent of the cylinder, a cylindrical wedge was simulated by imposing a rotational symmetry $n_{sym} = 20$ for $\eta = 0.909$. This gives an azimuthal extent at midgap of $1.05\pi d$. The axial box size was also minimal, Γ was set to $\Gamma = 2\pi/3$ for all simulations, meaning that a single Taylor roll pair could fit in to the domain. Simulating more than one roll was shown to be unnecessary for producing accurate results for the torque by Brauckmann & Eckhardt (2013). Furthermore, very sharp dropoffs of the axial spectra can be seen in Dong (2007) for wavelengths larger than one roll.

Full details of the numerical simulations are presented in Table 1. To demonstrate that our small boxes are sufficient, we refer the reader to Section 3.4, which show that the boxes are large enough for the autocorrelations to change sign in both axial and azimuthal direction. As previously mentioned, the azimuthal (streamwise) correlations decay much faster than those of PC flow, and thus smaller boxes can be used. The axial and azimuthal spectra shown in section 3.5 demonstrate that the mesh is sufficient to capture the small scales. We mention that $\Delta z^+ \approx 5$ is a marginally resolved case, while for the azimuthal direction, coarser resolutions can be used without loss of accuracy.

The simulations were run for about 100 large eddy turnover times based on $\tilde{t} = d/U_i$, after transient behaviour had died out. In time units based on the frictional velocity u_τ and half the gap width, this is between 3 and 4 turnover times. This might seem small

Case	Re_s	N_θ	N_r	N_z	Δx^+	Δz^+	Nu_ω	$Re_{\tau,i}$	Line colour
R1	$1 \cdot 10^5$	1024	1024	2048	9.1	2.7	69.5 ± 0.2	1410	Light blue
R2	$2 \cdot 10^5$	1536	1536	3072	11.4	3.4	126 ± 2.1	2660	Black
R3	$3 \cdot 10^5$	1536	1536	3072	16.8	5.1	171 ± 2.5	3920	Red
AF	$1 \cdot 10^5$	1024	1024	2048	9.1	2.7	66.2 ± 0.5	1390	Green

Table 1: Details of the numerical simulations. The first column is the name with which the simulation will be referred to in the manuscript. The second column is Re_s , the shear Reynolds number. The third to fifth columns represent the amount of points in the azimuthal, radial and axial directions, while the sixth and seventh columns show the resolution in inner wall-units at the mid-gap, $x = \frac{1}{2}(r_i + r_o)\Delta\theta$. The eighth column is the non-dimensional torque Nu_ω , and the ninth column is $Re_{\tau,i} = u_{\tau,i}d/(2\nu)$, the frictional Reynolds number at the inner cylinder. $Re_{\tau,o}$ can be obtained from $Re_{\tau,o} = \eta Re_{\tau,i}$. The AF case has an imposed axial flow with a mean velocity $U_w = \frac{1}{10}r_i\omega_i$. The final column shows the color code used for that simulation for Figures 3, 5, 6 and 8-10.

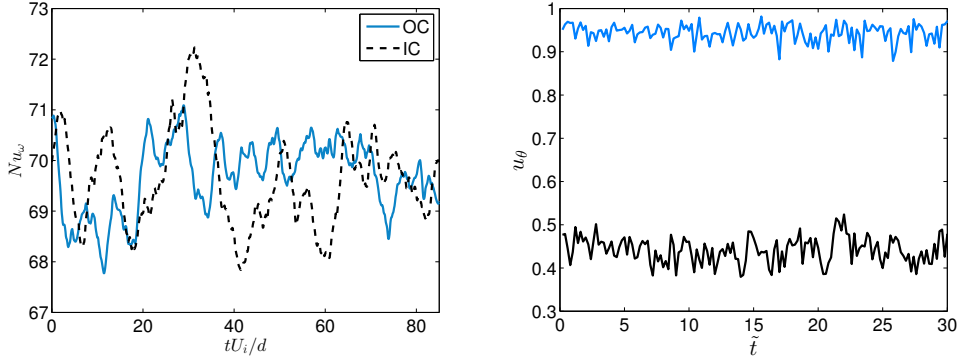


Figure 1: Left: Instantaneous Nu_ω at inner (IC) and outer (OC) cylinders for the R1 simulation. Right: instantaneous azimuthal velocity near the inner cylinder (blue) and in the mid-gap (black) for the R2 simulation. The temporal origin is arbitrary. Fluctuations are on timescales of the order $\mathcal{O}(d/U_i)$.

when comparing to channels, but it is sufficient for TC flow with pure inner cylinder rotation. The characteristic time for TC appears to be d/U_i . Dong (2008) already showed the decay of temporal autocorrelations in TC to happen in $\tilde{t} \approx 3$. This fast time scale is further quantified in the left panel of Figure 1, which presents the instantaneous torque, non-dimensionalized as a quasi-Nusselt number $Nu_\omega = T/T_{pa}$ for the R1 simulation, where T is the torque and T_{pa} is the torque in the purely azimuthal, laminar state, and the right panel of Figure 1, which shows the instantaneous azimuthal velocity at two points for the R2 case.

As we will see in more detail in Section 3.5, the Reynolds stresses which transport angular velocity are mainly localized in low-wavelength eddies, which have velocities of order $\mathcal{O}(U_i)$. This is not the case in channel flow, where the largest eddies are inactive,

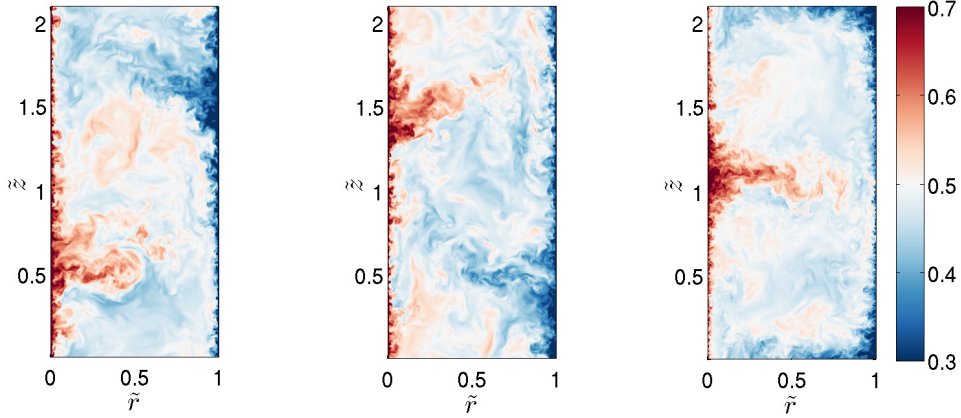


Figure 2: Visualization of the instantaneous azimuthal velocity u_θ for an azimuthal cut for the AF case at times separated by $t = 10$ (left and middle) and for the R2 case (right). The large scale pattern can be clearly seen all panels. The roll in the left and middle panels is slightly bent upwards due to the presence of an axial mean flow.

i.e. they do not transport Reynolds-stresses (Townsend 1976; Hoyas & Jiménez 2006). Reynolds-stresses are transported by boundary layer detachments, or streaks, with velocity scales of $\mathcal{O}(u_\tau)$, which then naturally leads to the time scales $\mathcal{O}(d/u_\tau)$ for shear transport. However, for the large scales to saturate in energy, much larger times are needed. Large scales are “fed” by detachments from the boundary layers with velocity $\mathcal{O}(u_\tau)$. This means that the *transients* in TC flow have time scale $\mathcal{O}(d/u_\tau)$.

3. Results

3.1. Visualization of the effect of pressure gradient

As mentioned previously, we have attempted to weaken the rolls by the addition an axial pressure gradient, such that a mean axial flow $U_w = \frac{1}{10}r_i\omega_i$ was sustained (case AF in Table 1). Figure 2 shows a pseudocolor plot of the instantaneous azimuthal velocity for the R2 case, and the AF case in two separate instances in time. The large scale patterns caused by the presence of an underlying Taylor-roll can be appreciated in all the panels. This roll is stationary in time in the case of the R2 simulation. For the AF case, the mean axial velocity satisfies $u_\tau \ll U_w \ll U_i$, but it does not prevent the formation of the Taylor rolls. Instead, it is slowly convected upwards in the computational domain, reappearing on the other side due to the axial periodicity. The formation of Taylor rolls appears to be inevitable, and this happens by the merging of the boundary layer detachments- the hairpin vortices.

3.2. Mean velocity profiles

The top two panels of Figure 3 show the mean azimuthal velocity profiles at the inner and outer cylinder, in wall units for all cases. Inner cylinder wall units are defined using $u_{\tau,i}$ as a velocity scale and $\delta_{\nu,i} = \nu/u_{\tau,i}$ as a length scale. The mean azimuthal profile is defined as a velocity difference, i.e. $U^+ = (U_i - \langle u_\theta \rangle_{t,z,\theta})/u_{\tau,i}$, where $\langle \phi \rangle_{x_i}$ denotes the variable ϕ averaged with respect to x_i . r^+ is the distance to the inner cylinder $r^+ = (r - r_i)/\delta_{\nu,i}$. Outer cylinder wall units are defined using $\delta_{\nu,o}$ and $u_{\tau,o}$, and $r^+ = (r_o - r)/\delta_{\nu,o}$. Inner and outer cylinder wall units use different scales. The outer cylinder branch is always

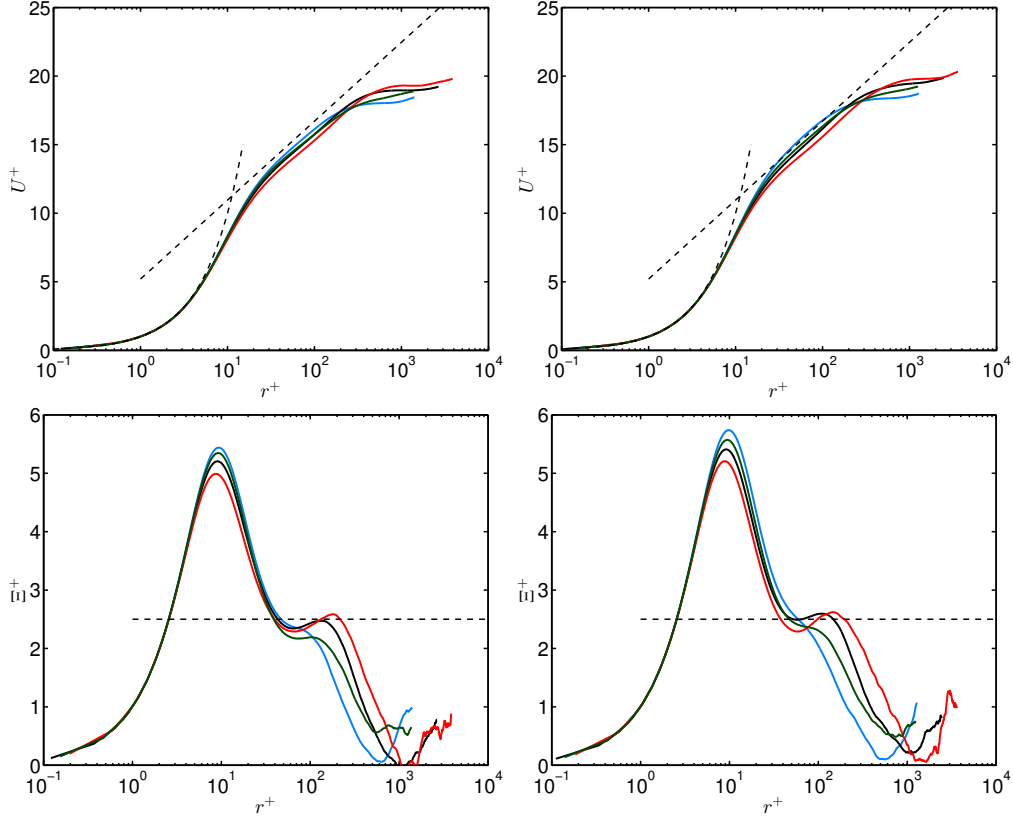


Figure 3: The two top panels show the mean azimuthal (streamwise) velocity profile at the inner (left) and outer (right) cylinders in wall units. Dashed lines are $u^+ = r^+$ and $u^+ = 2.5 \log(r^+) + 5.2$. The bottom panels show the logarithmic diagnostic function Ξ^+ at the inner (left) and outer (right) cylinders. The dashed straight line corresponds to $\Xi^+ = 2.5$ on both panels. Colours are as in Table 1.

slightly above than the inner cylinder branch, because the $u_{\tau,i} \approx \eta u_{\tau,o}$, and thus U^+ at the mid-gap is larger in outer cylinder wall units.

Very large deviations from the classic law-of-the-wall with von Karman constants of $\kappa = 0.4$ and $B = 5.2$ are seen. This can be also appreciated in the bottom two panels of Figure 3, which show the logarithmic diagnostic function

$$\Xi^+ = r^+ dU^+ / dr^+. \quad (3.1)$$

If U^+ is logarithmic, Ξ^+ should be horizontal and equal to the inverse of κ . For channels, deviations from the universal von Karman law were proposed by Jiménez & Moser (2007) and based on the overlap arguments of Afzal & Yajnik (1973) to have the following shape:

$$\Xi^+ = \kappa^{-1} + \alpha y/h + \beta Re_\tau^{-1/2}, \quad (3.2)$$

where h is the channel half-gap, and $\alpha = 1$ and $\beta = 150$ are obtained from fits to the data. Bernardini *et al.* (2014) found the data up to $Re_\tau = 4000$ to fit well to this equation, with slightly modified constants. For PC, Pirozzoli *et al.* (2014) were not able to quantify the deviations of Ξ^+ in a systematic way.

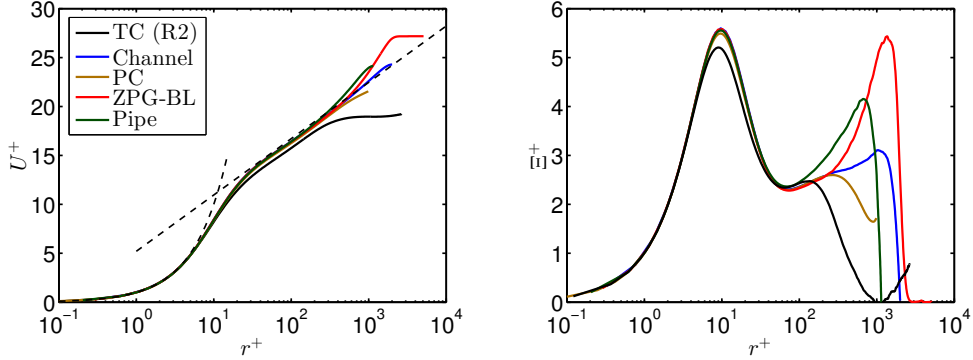


Figure 4: Left panel: mean streamwise component for several canonical flows. Right panel: Ξ^+ for the same flows. Legend: R2 case (black line), ZPG-BL at $Re_\tau \approx 2000$ from Sillero *et al.* (2013) (red), channel from del Álamo & Jiménez (2003) at $Re_\tau \approx 2000$ (blue), pipe flow data at $Re_\tau \approx 1100$ from Wu & Moin (2008) (dark green) and PC data at $Re_\tau \approx 1000$ from Pirozzoli *et al.* (2014) (yellowish-brown).

In the case of TC, fitting an equation similar to equation (3.2) to our DNS data in the logarithmic region does not lead to a good description of the data, as the effect of curvature and of the Taylor rolls is of extreme importance. A tilted S-like behaviour in Ξ^+ around $r^+ \approx 100$ can be appreciated for the R2 and R3 cases, which is very similar to the one seen in PC by Pirozzoli *et al.* (2014). When comparing the cases, there is still a strong dependence on Re_τ of the inner layer. The peak in Ξ^+ at $r^+ \approx 10$ is far from universal across our four simulations, and is probably due to the presence of the large scale structures. Our DNS data for TC at $\eta = 0.909$ are clearly insufficient to conclude anything about the deviations of Ξ^+ .

A “bending” of the profiles away from the logarithmic law is seen in the bulk for all simulations. This is especially significant from $r^+ > 500$. For $\eta = 0.909$, this corresponds to one tenth of the gap, or only 1% curvature. Even if 1% curvature is small, it is consistent with the notion that curvature plays a surprisingly large effect, and thus we may take $r^+ \approx 0.1Re_\tau$ as an upper bound for the log-layer in TC for $\eta = 0.909$. This means that the effective Re_τ of the simulations decreases substantially, and the possible logarithmic regions extend less into the bulk. Higher Re_τ are needed in TC to see the same profiles as in channels or pipes. This is shown in more detail in Figure 4, which compares the streamwise mean profile and Ξ^+ in several canonical flows. TC shows very large variability in Ξ^+ when compared to the other canonical flows.

If one takes the start of the logarithmic layer to be approximately at $r^+ = 3Re_\tau^{1/2}$ (Marusic *et al.* 2013), and curvature effects to be dominant at $r^+ \approx 0.1Re_\tau$, the range of validity of the assumptions made to obtain a logarithmic layer is reduced to $150 < r^+ < 400$, a clearly insufficient separation of scales to see a well-developed profile. Therefore, we cannot conclude anything about the mean azimuthal profile, even if we may speculate based on experimental results (Huisman *et al.* 2013) that further DNS at larger Re_τ will lead to the development of a region with properties consistent with those of other canonical flows.

3.3. Velocity and pressure fluctuations

Figure 5 shows the velocity and pressure fluctuations at the inner cylinder. The fluctuations, i.e. the root mean squared (rms) of a field ϕ is computed as $\phi' = [\langle \phi^2 \rangle_{\theta,t} -$

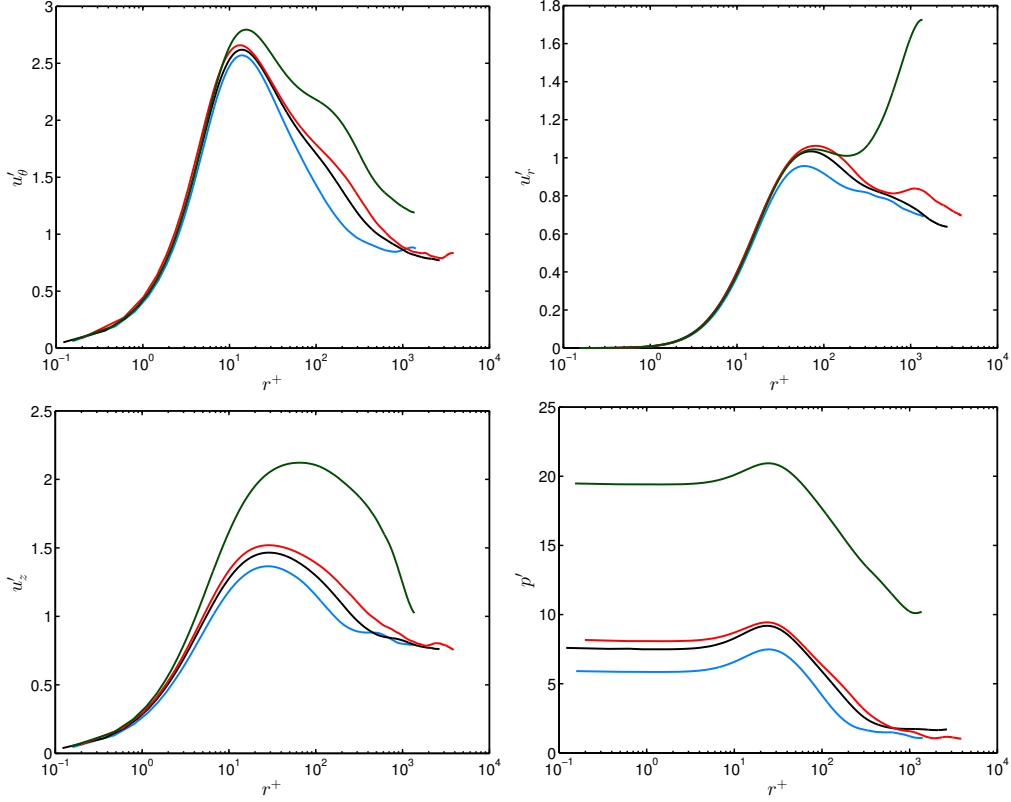


Figure 5: Mean fluctuation profiles for velocities and pressure at the inner cylinder in wall units. Colours are as in Table 1.

$\langle \phi \rangle_{\theta,t}^2 \rangle_z]^{1/2}$. The axial average and the subtraction operations must be computed in a precise order, due to the signature of the static large scale structures on the mean fields.

The velocity fluctuations are generally lower than those seen for channels and PC flow at comparable Re_τ . Except for the AF case, there is no presence of a second peak, and the level of fluctuations slightly increases with Re_τ , as expected. Velocity fluctuations are also shown in outer units in Figure 6. A reasonable collapse can be seen in an “overlap” layer. This layer is defined between $\tilde{r} < 0.2$, i.e. $r^+ < 0.4Re_\tau$, and $r^+ > 100$. In this region, u'_θ and u'_z show a small region which is consistent with logarithmic behaviour. This opens the door for the possibility of a region where overlap arguments are valid in TC. However, DNS with larger Re_τ is needed to sufficiently decouple the scales, and obtain a convincing overlap layer with logarithmic profiles in the fluctuations.

The addition of an axial flow greatly increases the level of fluctuations, especially those of the radial and axial velocities. A second peak in u'_θ for high r^+ can be seen to form, and the maximum values of u'_r and u'_z becomes much larger, especially in the bulk. These results are probably due to a combined effect of the axial flow and the large scale rolls, and can be discounted.

It seems that the Taylor rolls dampen fluctuations by fixing the position of the plume ejection regions. This is further quantified on Figure 7 which compares the streamwise fluctuations for the R1 and AF cases with those of several canonical flows at around $Re_\tau \approx 1000$. Except for PC and the R1 case, a remarkable agreement in the value of u'

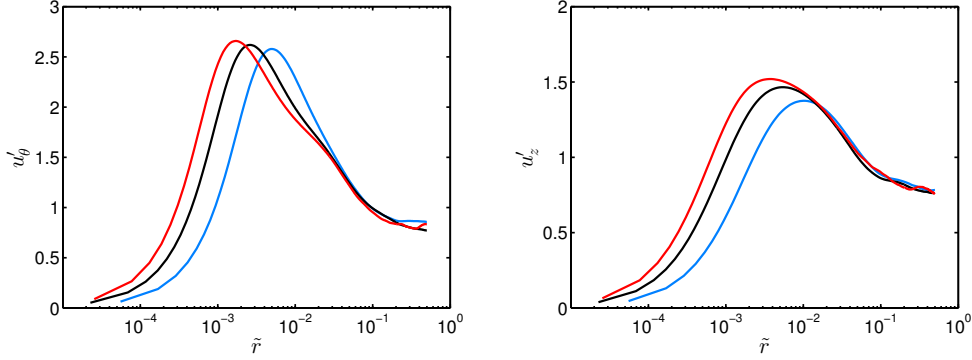


Figure 6: Fluctuations of the azimuthal (left) and axial (right) velocity components for R1, R2 and R3 cases in outer units. An overlap region, where the fluctuations collapse can be seen in the panel. Colours are as in Table 1

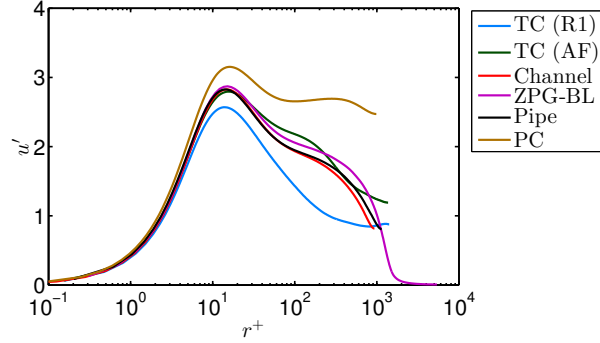


Figure 7: Streamwise velocity fluctuations for several canonical flows. Legend: R1 case (blue line), AF case (dark green), ZPG-BL at $Re_\tau \approx 1300$ from Sillero *et al.* (2013) (purple), channel from del Álamo & Jiménez (2003) at $Re_\tau \approx 950$ (red), pipe flow data at $Re_\tau \approx 1100$ from Wu & Moin (2008) (black) and PC data at $Re_\tau \approx 1000$ from Pirozzoli *et al.* (2014) (brownish yellow).

at the peak of $r^+ \approx 12$ is obtained, including the data from the AF case. The R1 case has a lower amount of fluctuations than the rest of the cases, again due to the constraints imposed by the fixed Taylor rolls.

Finally, we note that clear logarithmic behaviour is also seen in the overlap layer region for p' in Figure 5, and a collapse in the overlap region also happens between the R2 and R3 cases.

3.4. Axial and azimuthal autocorrelations

Figure 8 shows the autocorrelations for the azimuthal ($R_{\theta\theta}$) and radial (R_{rr}) velocities at the mid-gap. As mentioned previously, the azimuthal extent of the domain is sufficient, as it is large enough for the autocorrelation to change sign. This happens between 0.5 and 1 gap widths for all cases. This fast decorrelation is consistent with the finding that small computational boxes can obtain accurate results for the torque in TC, and is in contrast to PC, where azimuthal decorrelations take place in a length scale which is one order of magnitude larger, which leads to the necessity of large computational boxes are

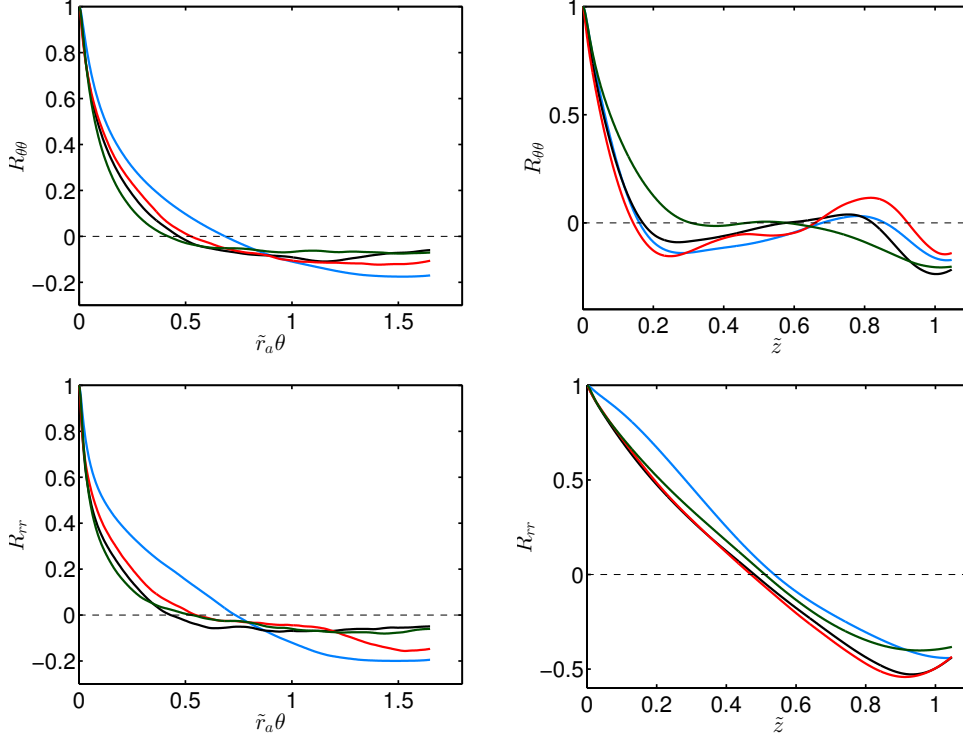


Figure 8: Autocorrelation functions for the azimuthal and radial velocities in the azimuthal and axial directions at the midplane $\tilde{r} = \tilde{r}_a$. The azimuthal extent of the computational boxes can be seen to be enough. The signature of the Taylor rolls can be seen on the axial autocorrelations for all cases. Colours are as in Table 1

needed (Bech *et al.* 1995; Tsukahara *et al.* 2006). The large scale Taylor roll has a clear signature on the axial autocorrelations $R_{\theta\theta}$ and especially R_{rr} . The presence of a roll can be inferred for all cases. Again we see that the axial pressure gradient does not weaken the roll, it only convects the whole structure.

3.5. Velocity power spectra

Taylor rolls contain a significant amount of energy, both in the bulk and in the boundary layer. Figure 9 shows the azimuthal and axial spectra near the wall, for $r^+ \approx 12$. The low-wavelength signature of the Taylor rolls is apparent in the axial spectra. This signature is not only present for $\Phi_{\theta\theta}$ and Φ_{zz} , but also for the radial velocity spectra Φ_{rr} for all cases. All cases show a maximum in the cospectra $\Phi_{\theta r}$ corresponding to $k_\theta = 0$, $k_z = 2\pi/\lambda_{TR}$, i.e. the wavelength of axisymmetric Taylor rolls. The rolls dominate the convective transport of angular velocity through the Reynolds stresses in the boundary layer. This means that Taylor rolls are not inactive in the sense of Townsend (1976) and Hoyas & Jiménez (2006), they *actively* transport angular velocity. Unlike the large scale structures in channel flow and PC flow, the rolls may be considered to be “attached” to the wall.

It might seem strange that such a large wavelength appears with the radial (wall normal) velocity near the wall, considering the impermeability condition. In channels and PC, the large scale structures reflect on the streamwise velocity near the wall. In TC, a

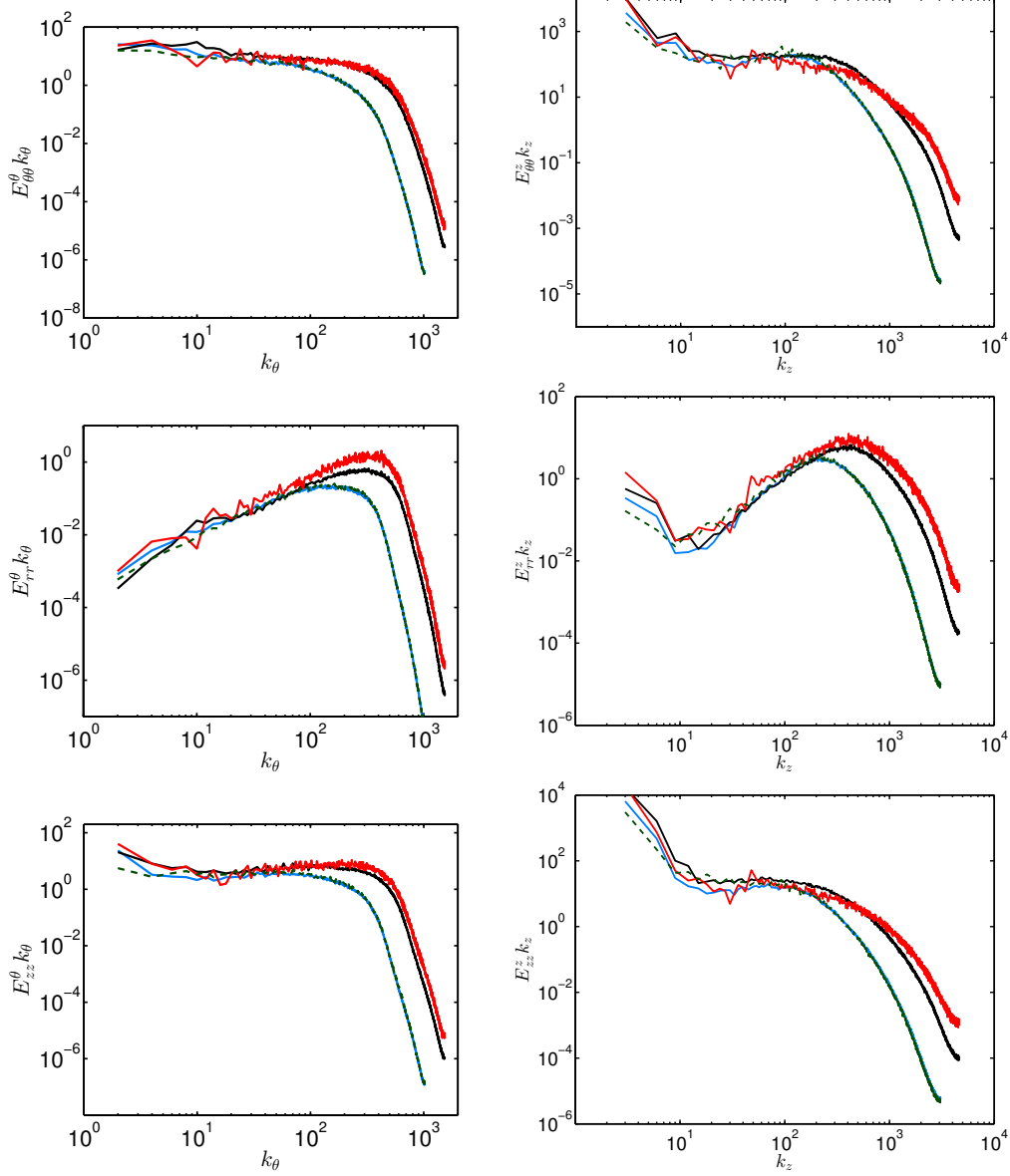


Figure 9: Azimuthal (left) and axial (right) spectra for all three velocity components for all simulations at $r^+ \approx 13$. Colours are as in Table 1.

perturbation of locally larger azimuthal (streamwise) velocity is linearly unstable, and will gain radial velocity. Therefore, one might think of the rolls as causing a large wavelength pattern in the azimuthal velocity near the walls, which causes a locally larger formation of hairpin vortices which have radial velocity, and this reflect back on the spectra. This is due to the fundamental difference between PC and TC, the linear instability.

As they form, the hairpin vortices, just like thermal plumes in thermal convection Eckhardt *et al.* (2007) tend to attract each other, and to merge, forming larger structures. The merging of the vortices is very apparent if the system is started from zero velocity initial conditions. The merging of the hairpin vortices forms the Taylor rolls in the bulk.

Rolls dominate the spectra at the mid-gap, shown in Figure 10. A prominent sawtooth behaviour in the axial spectra can be seen for the lowest wavenumbers. The spectra are consistent with the experiments by Lewis & Swinney (1999), and neither show -1 nor $-5/3$ scaling. This is unlike the case of pipe flow (Perry *et al.* 1986), for which a -1 scaling was found, and also unlike the case of curved channel flow (Hunt & Joubert 1979), which show the expected -1 scaling laws for the streamwise energy spectra in the streamwise direction. Also, the axial velocity spectra in the azimuthal direction do not show a $-5/3$ exponent which could be expected from Perry *et al.* (1986).

As noticed already by Brauckmann & Eckhardt (2013), the large-scale structures are responsible in TC for the transport of angular velocity, while the fluctuations transport on average very little, even though their instantaneous transport can be orders of magnitude higher than the mean transport (Huisman *et al.* 2012). Unlike in channel flow, and curved channel flow, the Reynolds stresses in TC are maximal at the mid-gap to satisfy the conservation of angular velocity current (torque). In PC, large scale structures also form, but these are also inactive, i.e. they do not transport shear (Avsarkisov *et al.* 2014). Therefore, it seems that small gap TC flow is the only flow examined up to date which involves transport by Reynolds stresses of a conserved quantity, in this case angular velocity, by large scale structures which are attached to the wall.

4. Summary and outlook

A series of large DNS simulations of small gap Taylor-Couette flow were conducted, reaching frictional Reynolds numbers of $Re_\tau = 4000$. Large scale structures, known as Taylor rolls form, and to play an active role in the system dynamics. Taylor rolls are present the bulk, and also are “attached” to the cylinders. They play an active role, by transporting angular velocity through Reynolds stresses. Even deep inside in the boundary layers, for $r^+ \approx 12$, their signature is significant in the $\phi_{\theta r}$ cospectra. Adding an axial pressure gradient was found to convect them slowly, but not to weaken them significantly. Their signature was still present in axial spectra in the boundary layer, and in the axial correlations of radial velocity.

The mean velocity profile of TC has significant differences from the Prandtl-von Karman log-layer profile $u^+ = \kappa^{-1} \ln y^+ + B$ with $\kappa \approx 0.4$ and $B \approx 5.2$. Large deviations for the logarithmic law are found even for 1% curvature, consistent with the notion that curvature effects are orders of magnitude larger than expected by mere dimensional analysis (Bradshaw 1973). Fluctuation profiles were also analysed, and the presence of rolls was found to reduce the level of fluctuations. When adding a mean axial flow, the azimuthal velocity fluctuations presented coincide with those seen in other canonical flows at comparable Re_τ . The velocity fluctuations were found to collapse in outer units, indicating the presence of an overlap region. Based on these findings, we expect that simulations at higher Re_τ will provide enough decoupling of scales for a large enough overlap region to form, and logarithmic profiles to form in both the mean azimuthal velocity, and the axial and azimuthal fluctuations.

Further investigations should also look at the effect of strongly counter-rotating cylinders, which have a Rayleigh-stable region, and how this region affects the large scale structures. Furthermore, in Ostilla-Monico *et al.* (2014b), it was found that large gaps, i.e. small η , severely weakens the rolls. Additional simulations at η around 0.5 provide more data on how the large scales interact with the boundary layers.

Acknowledgments: We would like to thank E. P. van der Poel for various stimulating discussions. RO is financially supported by ERC. We acknowledge that the results of

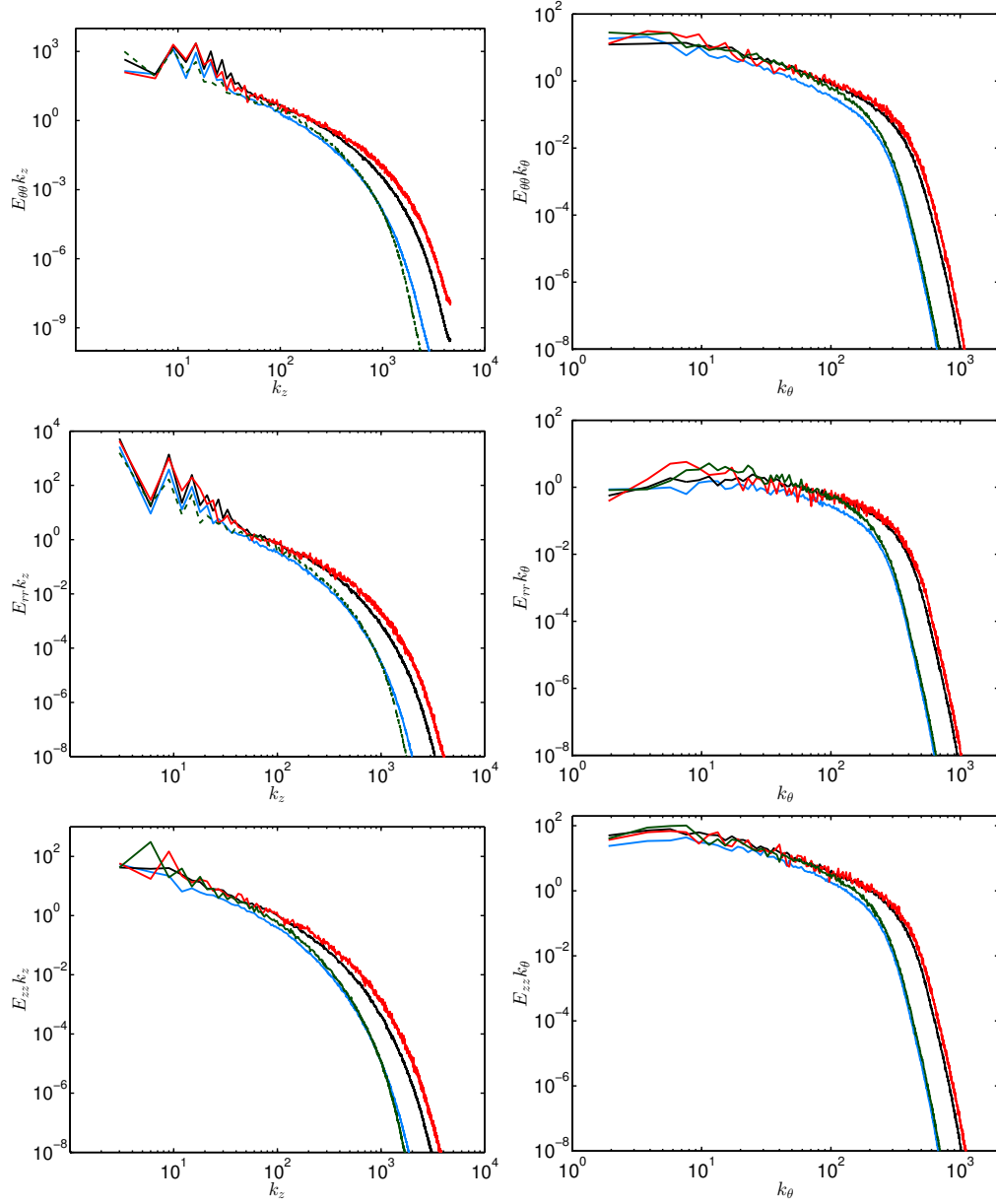


Figure 10: Azimuthal and axial spectra for all three velocity components for all simulations at mid-gap. Colours are as in Table 1.

this research have been achieved using the PRACE project 2013091966 resource CURIE based in France at Genci/CEA.

REFERENCES

- AFZAL, N. & YAJNIK, K. 1973 Analysis of turbulent pipe and channel flows at moderately large reynolds number. *J. Fluid Mech.* **61**, 23–31.

- DEL ÁLAMO, J. C. & JIMÉNEZ, J. 2003 Spectra of the very large anisotropic scales in turbulent channels. *Phys. Fluids* **15** (6), L41–L44.
- AVSARKISOV, V., HOYAS, S., OBERLACK, M. & GARCÍA-GALACHE, J. P. 2014 Turbulent plane Couette flow at moderately high Reynolds number. *J. Fluid Mech.* **751**, R1–8.
- BAILEY, S. C. C., VALLIKIVI, M., HULTMARK, M. & SMITS, A. J. 2014 Estimating the value of von Kármán's constant in turbulent pipe flow. *J. Fluid Mech.* **749**, 79–98.
- BECH, K. H., TILLMARK, N., ALFREDSSON, P. H. & ANDERSSON, H. I. 1995 An investigation of turbulent plane Couette flow at low Reynolds numbers. *J. Fluid Mech.* **286**, 291–325.
- VAN DEN BERG, T. H., LUTHER, S., LATHROP, D. P. & LOHSE, D. 2005 Drag reduction in bubbly Taylor-Couette turbulence. *Phys. Rev. Lett.* **94**, 044501.
- BERNARDINI, M., PIROZZOLI, S. & ORLANDI, P. 2014 Velocity statistics in turbulent channel flow up to $Re_\tau = 4000$. *J. Fluid Mech.* **742**, 171–191.
- BRADSHAW, P. 1973 The effects of streamline curvature on turbulent flow. *Tech. Rep.*. AGAR-Dograph no. 169.
- BRAUCKMANN, H. & ECKHARDT, B. 2013 Direct Numerical Simulations of Local and Global Torque in Taylor-Couette Flow up to $Re=30.000$. *J. Fluid Mech.* **718**, 398–427.
- CHOI, H., MOIN, P. & KIM, J. 1993 Direct numerical simulation of turbulent flow over riblets. *J. Fluid Mech.* **255**, 503–539.
- DONG, S. 2007 Direct numerical simulation of turbulent Taylor-Couette flow. *J. Fluid Mech.* **587**, 373–393.
- DONG, S. 2008 Turbulent flow between counter-rotating concentric cylinders: a direct numerical simulation study. *J. Fluid Mech.* **615**, 371–399.
- ECKHARDT, B., GROSSMANN, S. & LOHSE, D. 2007 Torque scaling in turbulent Taylor-Couette flow between independently rotating cylinders. *J. Fluid Mech.* **581**, 221–250.
- FAISST, H. & ECKHARDT, B. 2000 Transition from the Couette-Taylor system to the plane Couette system. *Phys. Rev. E* **61**, 7227–7230.
- VAN GILS, D. P. M., NAREZO-GUZMAN, D., SUN, C. & LOHSE, D. 2013 The importance of bubble deformability for strong drag reduction in bubbly turbulent Taylor-Couette flow. *J. Fluid Mech.* **722**, 317–347.
- HOFFMANN, P. H., MUCK, K. C. & BRADSHAW, P. 1985 The effect of concave surface curvature on turbulent boundary layers. *J. Fluid Mech.* **161**, 371–403.
- HOYAS, S. & JIMÉNEZ, J. 2006 Scaling of the velocity fluctuations in turbulent channels up to $Re_\tau = 2003$. *Phys. Fluids* **18**, 011702.
- HUISMAN, S. G., VAN GILS, D. P. M., GROSSMANN, S., SUN, C. & LOHSE, D. 2012 Ultimate turbulent Taylor-Couette flow. *Phys. Rev. Lett.* **108**, 024501.
- HUISMAN, S. G., SCHARNOWSKI, S., CIERPKA, C., KÄHLER, C., LOHSE, D. & SUN, C. 2013 Logarithmic boundary layers in strong Taylor-Couette turbulence. *Phys. Rev. Lett.* **110**, 264501.
- HUISMAN, S. G., VAN DER VEEN, R. C. A., SUN, C. & LOHSE, D. 2014 Multiple states in ultimate Taylor-Couette turbulence. *Nature Comm.* **5** (3820).
- HUNT, I. A. & JOUBERT, P. N. 1979 Effects of small streamline curvature on turbulent duct flow. *J. Fluid Mech.* **91**, 633–659.
- JIMENEZ, J. 2012 Cascades in wall-bounded turbulence. *Ann. Rev. Fluid. Mech.* **44**, 27–45.
- JIMÉNEZ, J. & MOSER, R. 2007 What are we learning from simulating wall turbulence? *Phil. Trans. R. Soc. Lond. A* **365**, 715–732.
- KIM, H. T., MOIN, P. & MOSER, R. 1987 Turbulence statistics in fully developed channel flow at low Reynolds number. *J. Fluid Mech.* **177**, 133–160.
- LEWIS, G. S. & SWINNEY, H. L. 1999 Velocity structure functions, scaling, and transitions in high-Reynolds-number Couette-Taylor flow. *Phys. Rev. E* **59**, 5457–5467.
- LOZANO-DURÁN, A. & JIMÉNEZ, J. 2014 Effect of the computational domain on direct simulations of turbulent channels up to $Re_\tau = 4200$. *Phys. Fluids* **26**, 011702.
- LU, J., FERNÁNDEZ, A. & TRYGGVASON, G. 2005 The effect of bubbles on the wall drag in a turbulent channel flow. *Phys. Fluids* **17**, 095102.
- MARUSIC, IVAN, MONTY, JASON P., HULTMARK, MARCUS & SMITS, ALEXANDER J. 2013 On the logarithmic region in wall turbulence. *J. Fluid. Mech.* **716**, R3.
- OSTILLA-MONICO, R., VAN DER POEL, E. P., VERZICCO, R., GROSSMANN, S. & LOHSE, D.

- 2014*a* Boundary layer dynamics at the transition between the classical and the ultimate regime of Taylor-Couette flow. *Phys. Fluids* **26** (015114).
- OSTILLA-MONICO, R., VAN DER POEL, E. P., VERZICCO, R., GROSSMANN, S. & LOHSE, D. 2014*b* Exploring the phase diagram of fully turbulent Taylor-Couette flow. *J. Fluid Mech.* **761**, 1–26.
- PERRY, A. E. & CHONG, M. S. 1982 On the mechanism of wall turbulence. *J. Fluid Mech.* **119**, 173–217.
- PERRY, A. E., HENBEST, S. & CHONG, M. S. 1986 A theoretical and experimental study of wall turbulence. *J. Fluid Mech.* **165**, 163–199.
- PIROZZOLI, S., BERNARDINI, M. & ORLANDI, P. 2014 Turbulence statistics in Couette flow at high Reynolds number. *J. Fluid Mech.* **758**, 327–343.
- SILLERO, J. A., JIMÉNEZ, J. & MOSER, R. D. 2013 One-point statistics for turbulent wall-bounded flows at reynolds numbers up to $\delta^+ \approx 2000$. *Phys. Fluids* **25**, 105102.
- TAYLOR, G. I. 1936 Fluid friction between rotating cylinders. *Proc. R. Soc. London A* **157**, 546–564.
- TOWNSEND, A. A. 1976 *The structure of turbulent shear flow*. Cambridge, UK: Cambridge University Press.
- TSUKAHARA, T., KAWAMURA, H. & SHINGAI, K. 2006 DNS of turbulent Couette flow with emphasis on the large-scale structure in the core region. *J. Turb.* **7** (19).
- VERZICCO, R. & ORLANDI, P. 1996 A finite-difference scheme for three-dimensional incompressible flow in cylindrical coordinates. *J. Comput. Phys.* **123**, 402–413.
- WU, X. & MOIN, P. 2008 A direct numerical simulation study on the mean velocity characteristics in turbulent pipe flow. *J. Fluid Mech.* **608**, 81–112.
- ZHU, X., OSTILLA-MÓNICO, R., VERZICCO, R. & LOHSE, D. 2015 Direct numerical simulations of Taylor-Couette flow with grooved cylinders. *In preparation* .